Available online at www.sciencedirect.com
ScienceDirect
Ceramics International 35 (2009) 479–486
CERAMICS INTERNATIONAL
www.elsevier.com/locate/ceramint

Synthesis of doped $Ba_{0.6}Sr_{0.4}TiO_3$ ceramic powder via a sol–freeze-granulation and freeze-drying process

F. Paul [a,b,*], J.R. Binder [a], H. Gesswein [a], H.-J. Ritzhaupt-Kleissl [a], J. Hausselt [a,b]

[a] Research Center Karlsruhe, Institute for Materials Science III, Hermann-von-Helmholtz-Platz 1, 76344 Eggenstein-Leopoldshafen, Germany
[b] IMTEK, University of Freiburg, Georges-Koehler-Allee 102, 79110 Freiburg, Germany

Received 15 October 2007; received in revised form 1 November 2007; accepted 3 January 2008
Available online 11 April 2008

Abstract

This paper presents a method for synthesizing undoped and doped ceramic (Ba,Sr)TiO_3(BST) powders. The method is based on a sol-drying process utilizing freeze-granulation and freeze-drying of freshly prepared sols. The presented route is flexible regarding the stoichiometry of the powders and the chemistry of the utilized doping agent. Starting materials are the alkaline-earth acetates and titanium isopropoxide. The used solvent is a mixture of glacial acetic acid and water. The resulting precursor powder exhibits spherical and highly porous granules. The microstructure of the granules shows cell-like structures with wall thicknesses in the range of 100 nm or less. The primary particle size can be varied between 40 nm and several hundred nm by simply varying the calcination temperature. At higher calcination temperatures the agglomerates are easier to destroy by ultrasonic treatment. The tested dopants were Fe^{3+}, Ta^{5+} and $Fe^{3+} + F^-$. The differently doped precursor and ceramic powders were examined using SEM-, TEM-, BET-, XRD- (with Rietveld-refinement), laser diffraction- and X-ray-fluorescence-techniques.

This method is well suited to provide variably and homogeniously doped precursors for the preparation of ceramic powders in the system BaO–SrO–TiO_2, which allows even the incorporation of fluoride anions and can be easily deagglomerated. Moreover codoping BST with Fe^{3+} and F^- has a significant impact on lattice spacings of the resulting ceramic powders.

Keywords: A. Drying; A. Powders-chemical preparation; A. Sol–gel processes; D. $BaTiO_3$ and titanates; Freeze-drying

1. Introduction

The system $Ba_{1-x}Sr_xTiO_3$ (BST) shows tunable behavior of its permittivity, when an electric dc-field is applied to it [1]. This opens up the field for a variety of potential applications in tunable radio frequency devices. Among these are phase shifters [2,3], tunable capacitors (varactors), tunable rf-filters to mention only some. These applications require the implementation of the device's functional part as a planar film. The films are usually integrated into the device with thicknesses below 500 nm using standard thin film processing techniques like physical vapor deposition or metal organic chemical vapor deposition. Both techniques require highly sophisticated and expensive equipment and furthermore show weakness in accurately controlling stoichiometry or dopants in the resulting films. Contrary to these thin film processing techniques screen printed thick-films of BST-, $BaTiO_3$(BT-) systems offer the possibility to process powders, already homogeneously incorporated with dopants. This may be achieved by the use of powders, derived from solution based, chemical methods like a modified sol–gel process.

Moreover screen-printing is an established processing technique in industry enabling the fabrication of thick film devices. Film thicknesses of 1 μm can be realized with this technique. Such small film thicknesses, however, require nanoscaled powders with homogeneously distributed dopants and narrow particle sizes. Doped powders with narrow particle size distributions, suitable for screen-printing films with a thickness of 2–3 μm can be provided by the described synthesis.

This article presents a variable preparation process for doped and nanoscaled BST-powders. These powders are derived through freeze-drying of acetate-based sols and are ready for the preparation of screen-printing pastes.

* Corresponding author at: IMTEK, University of Freiburg, Georges-Koehler-Allee 102, 79110 Freiburg, Germany.
E-mail address: florian.paul@imtek.uni-freiburg.de (F. Paul).

0272-8842/$34.00
doi:10.1016/j.ceramint.2008.01.014

2. Experimental

2.1. Sol preparation

The metal-organic precursors and ceramic powders were synthesized via an adapted sol–gel process based on the respective barium acetates (p.a., 99.0–102.0%, Merck, Germany) or strontium acetates ($0.5H_2O$, Reagent Grade, Aldrich, Germany) and titanium iso-propoxide ($>97\%$, Aldrich, Germany). In Fig. 1 an overview of the preparation process of the powders is presented. The acetates were dissolved in glacial acetic acid (p.a., 100%, Merck, Germany) at room temperature in a N_2 flooded reactor over night. The molar ratio of Ba to Sr was 6:4. To this clear solution the Ti isopropoxide was added at room temperature through a dropping funnel under vigorous stirring (1:1 molar ratio Ba/Sr:Ti). An exothermic reaction occured, the temperature rose to approximately 35 ° C and the solution kept being clear and colourless, but darkened very slightly. Right after the addition of the Ti-alcoholate ultrapure water (Millipore filtered, conductivity ≤ 0.54 μS) was added in such an amount, that diluted acetic acid with a mass content of 35% was created in the solvent and a mass ratio of 0.07 between the gelating starting materials (acetates and alcoholate) and the solvent (water and acetic acid) was obtained.

B-site dopants (Ta^{5+}-donor, Fe^{3+}-acceptor) and Fe^{3+}/F^{-}-acceptor–donor dopants on B-site and oxygen-site were incorporated either as water sensitive alcoholate (Tantalum(IV)-ethanolate 99,999% metals basis, Nb < 100 ppm, Alfa, Germany) or as water soluble nitrate ($Fe(NO_3)_3 \cdot 9H_2O$, Puratronic, 99,999%, metals basis, Alfa, Germany). The addition of acetates or hydroxides may be possible as well.

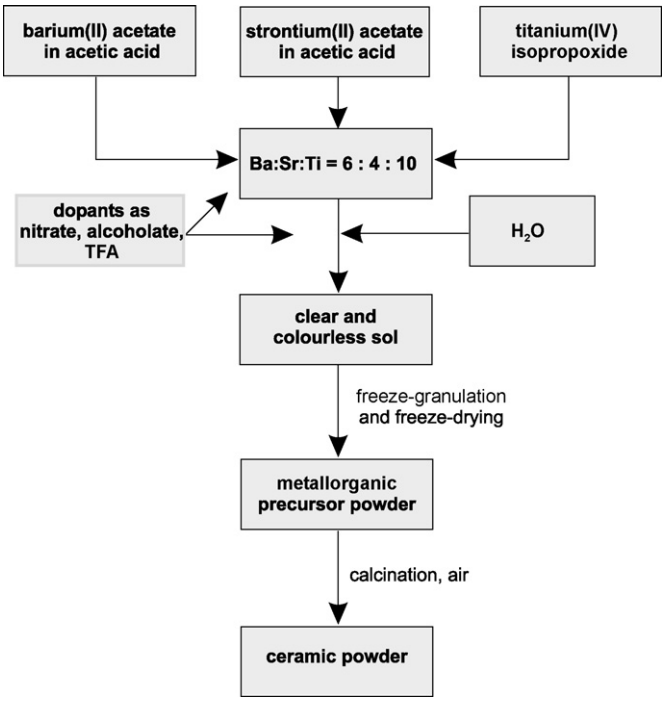

Fig. 1. Flowchart of the BST-synthesis.

Fluorine was added as trifluoroacetic acid (TFA, Uvasol for spectroscopy, Merck KgA, Germany).

The Ta-ethoxide has to be stabilized with 2,4-pentane-dione in a 1:1 molar ratio prior to addition to the solution of the Ba/Sr-acetates. $Fe(NO_3)_3 \cdot 9H_2O$ was dissolved in approximately 5 ml of water and was spilled with the remaining rest of the water into the reactor. TFA was added directly onto the dry Ba/Sr-acetates prior to the addition of acetic acid to facilitate coordinative bonding of TFA onto the Ba/Sr-cations.

2.2. Freeze-granulation

After dilution a water like solution was formed pH 3.5, which immediately after addition of the water was pumped directly from the reactor to the freeze-granulator and sprayed into liquid nitrogen to form frozen sol-granules. The spraying equipment consisted of a peristaltic pump (Watson-Marlow, 505 S) operated at an average 50 rpm, an elastic tube (Tygoon, R3603) with an inner diameter of 5.5 mm (allowing for a flow of approximately 2 ml/s), a N_2-powered spray nozzle (two component jet) made from stainless steel and a Dewar vessel with an inner diameter of approximately 21 cm. The vessel was equipped with a lid made from PVC, bearing the spray-nozzle and a Teflon-plated mechanical stirrer.

2.3. Freeze-drying

After spraying, the frozen sol-droplets, suspended in liquid nitrogen, were poured onto plates made out of stainless steel to form a layer of 1–2 cm thickness. These plates were put on heatable shelves and a Pt100 temperature sensor was placed in the frozen granules to be dried. The shelves were stacked in a fastener and placed in a laboratory freeze-dryer (Christ, Alpha 1–2). For freeze-drying the frozen granules were not heated for the first 96 h and sublimated at a pressure of approximately 0.002 h Pa only by heat radiation from the environment. After these 96 h the temperature of the granules had risen to 10 ° C and the shelves were manually heated in three steps (20 and 40 ° C for 1 h each) to 100 °C. After 1 h at 100 ° C the dried precursor-xerogel-granules were cooled by flooding the drying chamber with N_2. The precursor powder, still hot, was filled into containers made from PE. The morphology of the precursors was investigated by SEM (Leo 1530 Gemini).

2.4. Calcination of the precursor

The freeze-dried precursors were pyrolized (calcined) in alumina crucibles for 1 h at 700 ° C with a heating rate of 5 °C/min and a cooling rate of 10 °C/min. Alternatively the undoped precursor was calcined for 1 h at 900 and 1100 ° C with equal heating and cooling rates. The used furnace was a chamber furnace (Carbolite RHF1400) and the atmosphere was ambient air (flow 15 l/min) for the undoped, Fe-doped and Ta-doped precursors. The Fe/F-codoped precursor was calcined in a tube furnace (Heraeus CTF1600) under dried (by molecular sieve and P_2O_5) synthetic air. The nominal compositions of the powders prepared in this study are listed in Table 1.

Table 1
Nominal compositions of the prepared ceramic powders

Dopant(s)	Content	Nominal composition
–	Undoped	$Ba_{0.6}Sr_{0.4}TiO_3$
Fe	0.1% Fe	$Ba_{0.6}Sr_{0.4}Ti_{0.999}Fe_{0.001}O_3$
Fe	1% Fe	$Ba_{0.6}Sr_{0.4}Ti_{0.99}Fe_{0.01}O_3$
Ta	0.1% Ta	$Ba_{0.6}Sr_{0.4}Ti_{0.999}Ta_{0.001}O_3$
Ta	1% Ta	$Ba_{0.6}Sr_{0.4}Ti_{0.99}Ta_{0.01}O_3$
Fe, F	1% Fe + F^-	$Ba_{0.6}Sr_{0.4}Ti_{0.99}Fe_{0.01}O_{2.97}F_{0.03}$

2.5. Ceramic powders

The ceramic powders were characterized by SEM (Leo 1530 Gemini), TEM (Philips CM 200 FEG equipped with an EDX (non-calibrated)), X-ray diffraction (Bragg-Brentano set up) and Rietveld refinement, laser diffraction (Leeds & Northrup, Microtrac x100), FT-IR-spectroscopy (as pressed KBr-pellets in a Bruker IFS 28) and determination of the BET-surface (Micromeritics FlowSorb II 2300 & DeSorb 2300A). Powder X-ray diffraction patterns were recorded on a Siemens D5000$\theta/2\theta$ diffractometer (reflection geometry) by using Cu K $\alpha_{1,2}$ radiation with a secondary curved graphite monochromator. The diffractometer optic used was a fixed divergence slit of 1°, anti-scatter slit of 1° and a receiving slit width of 0.6 mm. The X-ray tube operated at 40 kV and 30 mA. Data were collected at room temperature in the 2θ range of 20– 120° with a step size of 0.02° and fixed counting times between 5 and 40 s per step.

The full-profile-fitting refinements were carried out by the Rietveld method using the program *FullProf* [4,5]. The background was fit by a six-parameter polynomial and refined simultaneously with the sample displacement, scale factors and cell dimensions. The modified Thomson–Cox–Hastings pseudo-Voigt profile function was used for the peak shape. The instrumental contribution to peak broadening was determined with annealed BaF_2powder as a standard material.

After characterization the powders were incorporated into screen-printing-pastes. To determine their composition, these pastes were poured into a crucible made from alumina and were sintered (equal to a common sintering profile) under ambient atmosphere at 1200 ° C for 1 h with a heating rate of 5 °C/min, in a Linn VMK 1400 chamber furnace. The cooling rate was 5 °C/min. The Fe/F^--codoped paste was sintered in a tube furnace (Heraeus CTF1600) under dried (by P_2O_5) synthetic air with the same temperature profile as mentioned above. The preparation of pastes, sintering of BST-thick-films and their influence on microstructure are published in a separate article [6].

The remaining ceramics were analyzed by X-ray fluorescence analysis (Bruker-AXS, SRS 303AS, Dr. C. Adelhelm, Institute for Materials Science I at Research Center Karlsruhe) using a borate matrix. The fluoride content was checked by gel-chromatography in conjunction with hydropyrolitic pulping (HC Starck GmbH, Goslar).

3. Results and discussion

3.1. Morphology of the precursor

The resulting precursor granules after freeze-drying exhibit spherical shapes with a very high degree of open porosity as illustrated in Fig. 2. Their specific BET-surface was 36 m^2/g and their apparent density was so small, that some problems were inflicted on transfilling the precursor powder quantitatively. Its shape derives from the sol-droplets created by spraying the sol into liquid nitrogen. Its size distribution is very broad and may be influenced by the spraying technique, e.g. ultrasonic spraying may provide a smaller size distribution of the granules.

The inner structure of the precursor-granules show ligament-like partition walls with a maximum thickness of about 100 nm. They are created by the precipitation of gel at the grain boundaries of water and acetic acid crystals during freezing of the solvent. Thus, the structure of the xerogel is heavily dependent on the crystallisation behavior of the solvent during freezing.

A gel-mass ratio of 0.07 and a sol-concentration of 35% acetic acid by weight turned out to reliably produce finely structured xerogel granules, even though acetic acid shows a pronounced freezing point depression upon dilution with water [7]. However, the structure of the xerogel-precursor is influenced by the concentration of the sol and acetic acid as

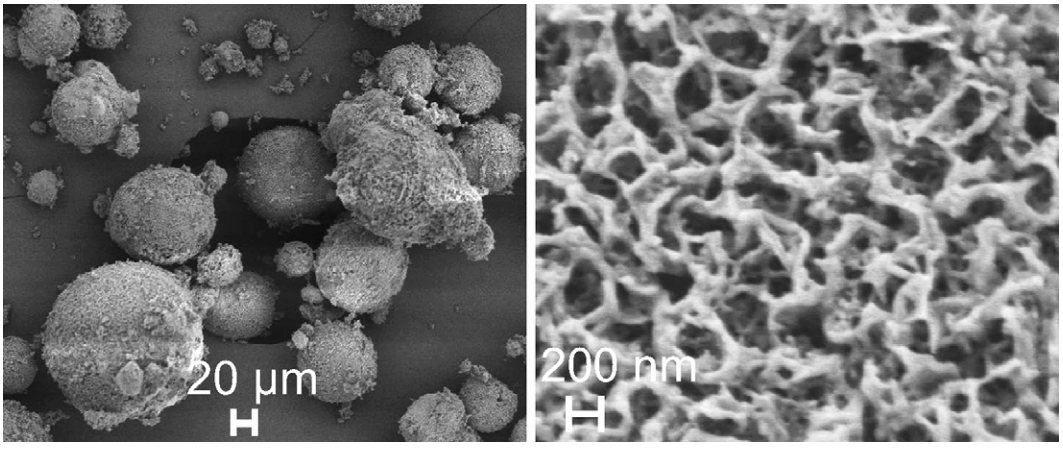

Fig. 2. SEM micrographs of undoped freeze-dried precursor granules.

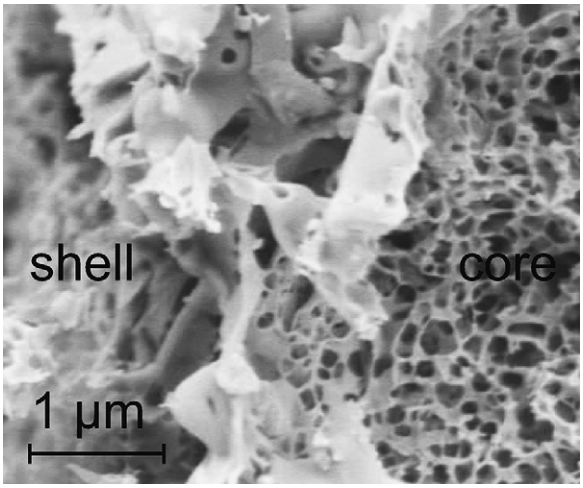

Fig. 3. SEM micrograph of the outer shell (coarse structure) and the inner core (fine structure) of an undoped freeze-dried precursor granule (fractured).

well as by the freezing- and drying-speed. For example freezing the sol-droplets (with the mentioned composition) in liquid nitrogen leads to granules with a finely textured structure in the core and a coarse structure in the shell as shown in Fig. 3. This very probably is caused by the so called Leidenfrost-phenomenon [8,9]. The results from further investigations of the factors influencing the morphologies of the resulting structures will be published in a future publication.

3.2. Morphology of the ceramic powder

After calcination of the precursor in the undoped state at 700 ° C for 1 h ceramic granules with structures similar to the precursor resulted (Fig. 4). SEM and TEM investigations reveal a primary particle size in the range from 30 nm to 50 nm (Fig. 4). The TEM images show crystallinity throughout the particle. No twinned crystals and no amorphous particles could be found. The observed electron diffraction patterns revealed a cubic structure in the crystals. Though some finely distributed and small areas of inhomogeneity could be found in some grains (Fig. 5). EDX-measurements revealed no significant difference between the inhomogeneities and the surrounding crystal (Fig. 5). As will be discussed in Section 3.4, these areas may be residual carbonate phase remaining from calcination.

3.3. Particle size variation and distribution of the ceramic powders

By variation of the calcination temperature the primary particle size of the undoped powders could be varied between about 40 nm at 700 °C, about 100 nm at 900 ° C and approximately 200 nm at 1100 ° C as can be seen in Figs. 4 and 6. Additionally to the increase of the grain size the particle size distribution broadens by increasing calcination temperature.

After calcination the powders calcined at 1100 ° C were easier to deagglomerate by ultrasonic treatment in acetone than

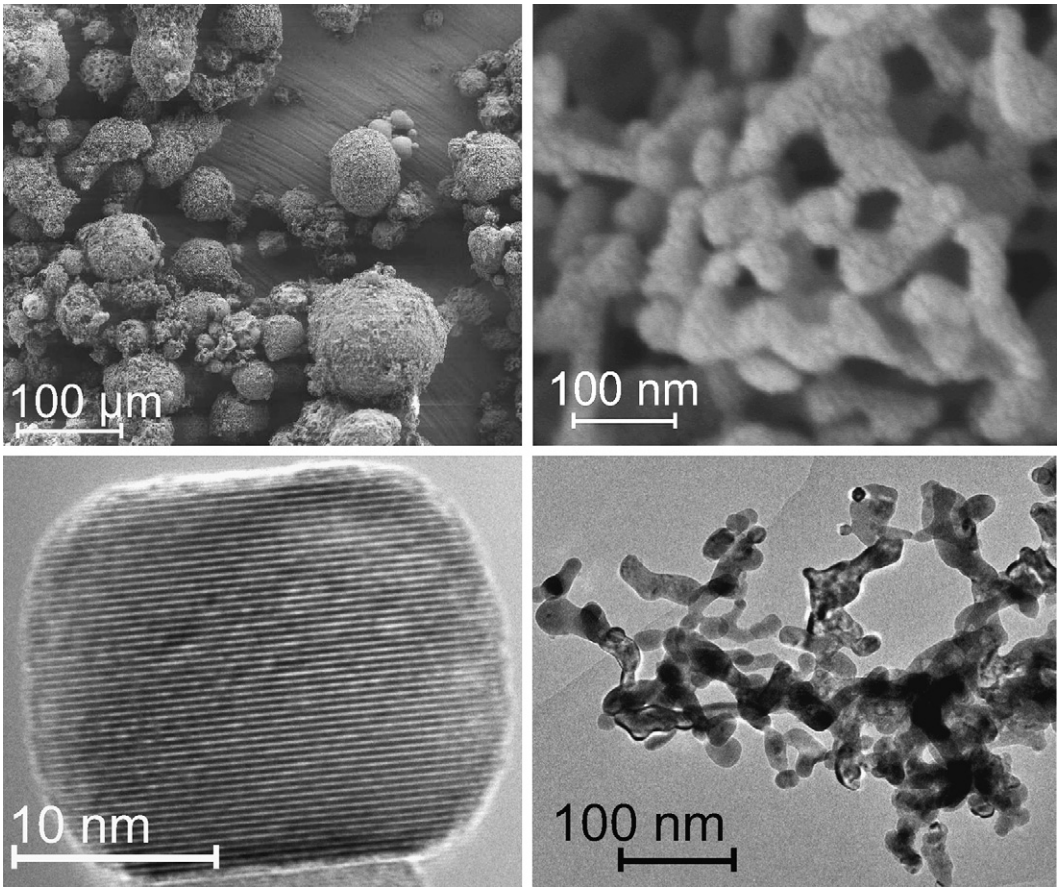

Fig. 4. SEM (above) and TEM (below) micrographs of undoped ceramic powder after 1 h calcination at 700 ° C under ambient air.

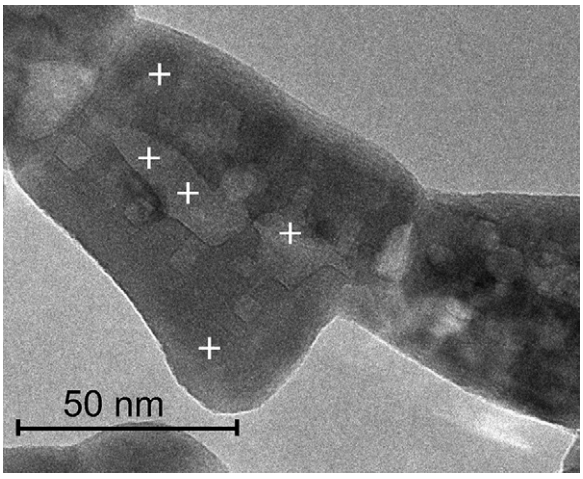

Fig. 5. TEM micrograph of an undoped crystallite with areas of visual inhomogeneity (1 h calcination at 700 ° C under ambient air). The crosses denote points of EDX measurements, with a spot size of approximately 10 nm.

the powders, which had been calcined at 700 °C. This can be seen in Fig. 7. The powder, which had been calcined at 1100 ° C shows no agglomerates with sizes bigger than 2 μm. The reason for this behavior is very probably due to the reduced number of grains and thus a reduced number of grain boundaries giving rise to a decreased stability.

The results of BET-measurements carried out on the different undoped and doped powders are listed in Table 2. The primary particle diameters of the agglomerates calculated from BET-surfaces ($d_{BET} = 6/(\rho A_{BET})$, assuming spheres, $\rho = 5683$ g/cm^3 ICDD powder diffraction file no. 34411) are a little higher than the ones estimated from SEM and TEM micrographs due to neck formation during calcination. The doped powders show slightly coarser particles than the undoped, which might be caused by melting effects during freeze-drying as well as by different sintering activities of the powders.

3.4. X-ray diffraction of the powders

Phase composition and crystallinity of the calcined powders at room temperature have been checked by X-ray diffraction and Rietveld refinement. The experimental diffraction patterns of all powders calcined at 700 ° C show diffraction peaks of $Ba_{0.6}Sr_{0.4}TiO_3$ as well as some weak and broad peaks of a residual carbonate phase. After calcination of the undoped powder at 1100 ° C this residual carbonate phase completely decomposed. This could be confirmed by FT-IR measurements.

To extract qualitative microstructural information from the broadened diffraction lines, the integral breadths β (uncorrected for the instrumental broadening) of several Bragg reflections of the BST powders were determined from an individual line profile analysis. The broadening caused by crystallite size and the broadening arising from local strain were separated according to the classical Williamson–Hall relation $\beta^* = 1/D + 2ed^*$ [11]. In a Williamson–Hall plot the reciprocal

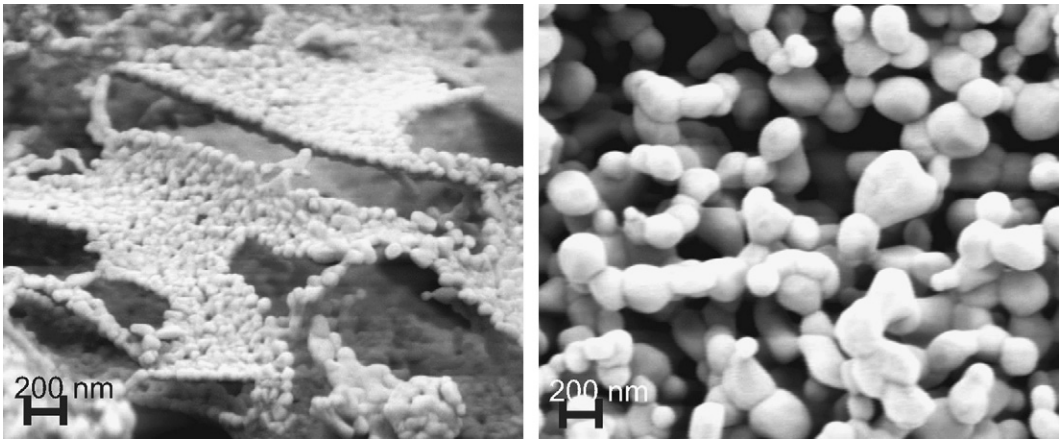

Fig. 6. SEM micrographs of undoped powder after calcination for 1 h at 900 ° C (left) and 1100 ° C (right).

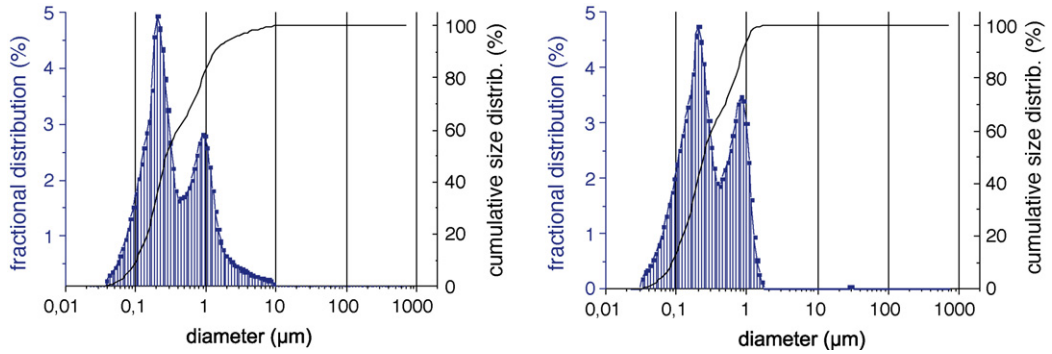

Fig. 7. (left) Particle size distribution of the calcined ceramic powder (1 h at 700 °C) after 240 min ultrasonic treatment. (right) 1 h at 1100 ° C calcined precursor after 240 min ultrasonic treatment in acetone. Measured by laser diffraction in 2-propanole.

Table 2
Specific surfaces (BET) and calculated particle sizes of the ceramic powders

Powder	Calcination conditions	BET-surface (m^2/g)	Diameter (nm)
Undoped	700 °C, 1 h	18.3	58
Undoped	1100 °C, 1 h	3.7	285
0.1% Fe	700 °C, 1 h	17.0	62
1% Fe	700 °C, 1 h	16.6	64
1% Fe + F	700 °C, 1 h	15.4	69
0.1% Ta	700 °C, 1 h	14.4	73
1% Ta	700 °C, 1 h	13.3	79

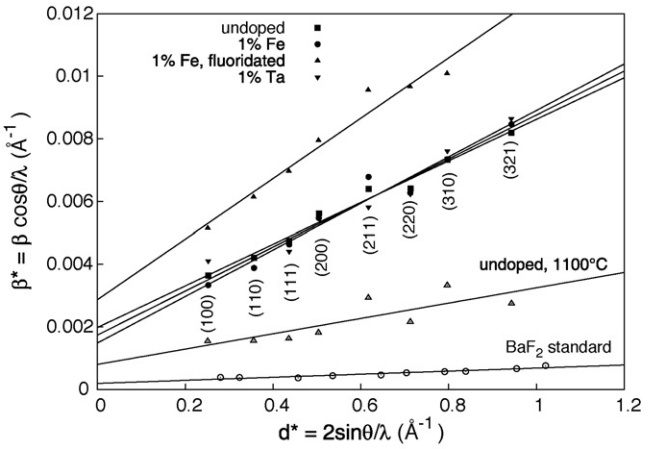

Fig. 8. Williamson–Hall plots (β^* vs. d^*, where $d^* = 1/d$) for the different BST powders and the BaF_2 standard.

integral breadth $\beta^* = \beta\cos\theta/\lambda$ is plotted as a function of reciprocal-lattice spacing $d^* = 2\sin\theta/\lambda$. The slope and intercept of the graph provide estimated values for the lattice strain e and the apparent crystallite size D [12]. In Fig. 8 the Williamson–Hall plot of the calcined powders and the BaF_2 standard are shown. All BST samples have a significant size contribution to line broadening and the non-zero slopes indicate the presence of strain broadening. Apparently the fluoridated powder exhibits a high degree of local strain indicating that the fluoride ions have been incorporated into the perovskite lattice. In contrast to all other powders the undoped powder, which had been calcined at an elevated temperature of 1100 ° C exhibits a significant smaller slope. This indicates little strain broadening, which may be due to an increased degree of crystal quality. Moreover, in this powder no significant size contribution to line broadening could be measured due to considerable grain growth.

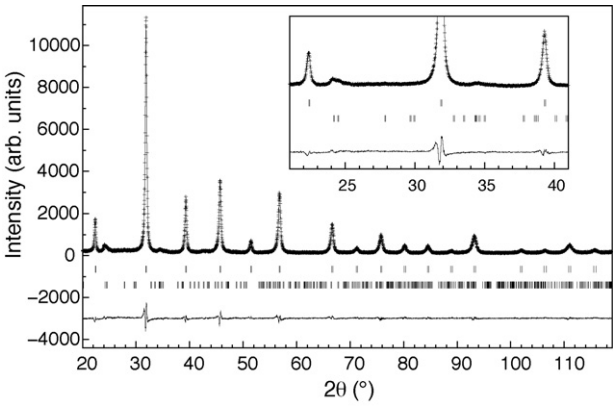

Fig. 9. Rietveld plot for undoped BST powder calcined at 700 °C. The vertical bars correspond to the positions of the Bragg reflexions of cubic BST and orthorhombic $(Ba,Sr)CO_3$. The inset shows an enlarged part of the fitting.

The observed profiles have to be corrected for instrumental broadening to allow for a more accurate determination of the average microstructural properties. Therefore, a line broadening analysis based on a whole-pattern fitting method as implemented in the *FullProf* program [5] was undertaken [13]. Rietveld refinements were carried out based on cubic $Ba_{0.6}Sr_{0.4}TiO_3$ (c-BST)with spacegroup $Pm\bar{3}m$ and orthorhombic $(Ba,Sr)CO_3$ (BC) with spacegroup *Pmcn*. The apparent volume-weighted size ϵ_β and upper-limit (maximum) microstrain values were obtained by the Rietveld refinements and the results of the phase analysis are listed in Table 3. As an example in Fig. 9 the observed, calculated and difference pattern of the undoped BST sample calcined at 700 ° C are plotted. The undoped, Fe- and Ta-doped BST samples have similar crystallite sizes and microstrains ranging from 42 to 48 nm and 34×10^{-4} to 36×10^{-4}, respectively. The fluoridated sample shows higher crystallite sizes of approximately 78 nm, significant higher microstrain of 62×10^{-4} and a higher amount of residual carbonate phase of 13 wt.%. This carbonate phase is probably very finely distributed throughout the BST crystals as already dicussed in Section 3.2. The diameters calculated from BET-surfaces as reported in Table 2 have the same order of magnitude as the diameters derived from X-ray diffraction and electron microscopy.

3.5. Stoichiometry of the powders

The results of the X-ray-fluorescence analysis and the calculated stoichiometries are listed in Table 4. The stoichiometries show little deviation from the nominal values.

Table 3
Characteristics of the BST powders (calcined 1 h at 700 °C) obtained by Rietveld refinement: lattice parameters, crystallite size, microstrain, existing crystalline phases and *R*-factors (%) of the refinements

Powder	a (Å)	ϵ_β (nm)	Microstrain, $e(\times 10^{-4})$	Crystalline phases	R_{wp} [R_{exp}]
Undoped	3.9695	46	35	c- BST + BC (6)	14.0 [8.7]
1% Fe	3.9691	48	34	c- BST + BC (6)	13.5 [8.6]
1% Fe + F^-	3.9704	78	62	c- BST + BC (13)	14.0 [8.7]
1% Ta	3.9704	42	36	c- BST + BC (4)	13.2 [5.5]

wt.% of BC ($(Ba,Sr)CO_3$) is given in parentheses.

Table 4
Results of the XRF-analysis of the ceramic powders incorporated into screen-printing-pastes and sintered 1 h at 1200 °C

Powder	Content (wt.%)						A-/B-site ratio	Ba/Sr ratio
	Ba	Sr	Ti	Fe	Ta	F		
Undoped	38.61	16.37	22.47	< 0.01	–	–	0.997	1.505
0.1% Fe	38.71	16.43	22.50	0.028	–	–	0.998	1.501
1% Fe	38.77	16.40	22.32	0.26	–	–	0.998	1.507
0.1% Ta	39.08	16.55	22.45	–	0.074		1.009	1.504
1% Ta	38.44	16.34	22.13	–	0.81	–	1.000	1.500
1% Fe + F^-	38.84	16.38	22.31	0.26	–	0.04	0.998	1.508

The A-/B-site ratios and Ba/Sr ratios have been calculated from these data and have been normalized in respect to the B-site (Ti-site). F^--content was checked by hydropyrolytic pulping and gel-chromatography.

However, a small Ba-surplus in the Ba/Sr-ratio can be detected as well as a slight excess on the B-site.

The difference between the nominal fluoride-content and the measured shows the volatility of the fluoride anion during thermal processing and the difficulties of precisely adjusting fluoride content. However, the chemical analysis together with the results from X-ray diffraction indicate that the fluoride has been incorporated into the perovskite lattice. It seems very likely, that it occupies oxygen vacancies, which have been created by the acceptor-dopant Fe. Yet, doubt remains about the place, where a possible surplus of fluorine goes to, which would exceed the nominal amount of dopant-created oxygen vacancies. This issue will be examined in future investigations.

4. Conclusion

A method for the synthesis of doped, nano-scaled ceramic BST-powders has been developed. It is based on freeze-granulation and freeze-drying of acetate based sols. The resulting ceramic powders can be doped with dopants of different type. The overall stoichiometry can reliably be adjusted. The choice of the dopant is not limited by the chemistry of its starting material, as acetates, nitrates or alkoxides may be used for incorporation of the dopants. Even the incorporation of fluoride ions by TFA is possible. However, the determined content of fluoride is not equal to the nominal content. The resulting powders show highly porous granules. Therefore this method might be also usefull for the generation of porous structures in medical or biological applications. The ceramic powders show agglomerated particles with primary particle sizes of around 40 nm. The agglomerates are very porous and weakly bound. They can be broken up to sizes below 2 μm by ultrasonic treatment alone and thus offer the possibility of a low degree of contamination with foreign elements during paste preparation. After a calcination temperature of 1100 ° C the agglomerates can be broken up even easier than after calcination at 700 °C.

The X-ray diffraction patterns of the ceramic powders after calcination for 1 h at 700 ° C showed broad peaks due to comparably small crystallite size. However, the fluoridated powder showed pronounced peak-broadening due to a considerable amount of lattice distortion. This is probably due to the intented incorporation of F^-anions on the oxygen site. The Goldschmidt factor [14,15] of these has been calculated using ionic radii after Shannon [16]. The high factor of 1.106 in Fe–F codoped BST, assuming a complete substitution of oxygen by fluoride and of titanium by iron, compared to the factor of undoped BST (1.062) suggests, that strain is induced by the introduction of Fe and F into the perovskite-lattice. These results should be supplemented by additional characterization methods in the future to make clear the whereabout and oxidation state of the introduced dopants.

Nevertheless, not only lattice parameters, but also dielectric properties of doped and undoped thick films show a strong influence of Fe and especially Fe/F codoping. Dielectric properties of thick films, prepared by the described method will be in the focus of a future publication.

The X-ray diffraction experiments also show that thermal treatment of the ceramic powders at elevated temperatures shows a measureable influence of calcination temperature on lattice distortion of undoped BST-powders. Their influence on dielectric properties will be discussed in a future publication, too.

References

[1] A.K. Tagantsev, V.O. Sherman, K.F. Astaviev, Ferroelectric materials for microwave tunable applications, J. Electroceram. 10 (2004) 1–62.
[2] F. Zimmermann, M. Voigts, C. Weil, Investigation of barium strontium titanate thick films for tunable phase shifters, J. Eur. Ceram. Soc. 21 (2001) 2019–2023.
[3] R. Babbitt, T.E. Koscica, W.C. Drach, L. Didomenico, Ferroelectric phase shifters and their performance in microwave phased array antennas, Integr. Ferroelectr. 8 (1995) 65–76.
[4] J. Rodriguez-Caraval, Recent advances in structure determination by neutron powder diffraction, Physica B 192 (1993) 55–69.
[5] J. Rodriguez-Carvajal, T. Roisinel, Line broadening analysis using Full-Prof: determination of microstructural parameters, Mater. Sci. Forum 443–444 (2004) 123–126.
[6] F. Paul, J.R. Binder, A. Berto, H.J. Ritzhaupt-Kleissl, G. Link, Influence of the process parameters on the microstructure of screen-printed $Ba_{0.6}Sr_{0.4}TiO_3$(BST60) thick-films on alumina substrates, in: Proceedings of the 2nd International Conference on Multi-Material Micro Manufacture (4M), Grenoble, France, September 20–22, (2006), pp. 221–229, ISBN: 0-08-045263-9.
[7] Chapter ethanoic acid, in: Monnier, Le, Kirk-Othmer (Eds.), Encyclopedia of Chemical Technology: Electron Tube Materials to Ferrites, vol. 8, 2nd ed., John Wiley & Sons, New York, 1965, pp. 386–404.
[8] J.G. Leidenfrost, On the fixation of water in diverse fire, Int. J. Heat Mass Transf. 9 (11) (1966) 1153–1166.
[9] W. Listerman, T.A. Boshinski, L.F. Knese, Cooling by immersion in liquid nitrogen, Am. J. Phys. 54 (6) (1986) 553–558.

[11] G.K. Williamson, W.H. Hall, X-ray line broadening from filed aluminium and wolfram, Acta Metall. 1 (1953) 22–31.
[12] C.H. Muller, F. Jacob, Y. Gagou, E. Elkaïm, Cationic disorder, microstructure and dielectric response of ferroelectric SBT ceramics, J. Appl. Crystallogr. 36 (2003) 880–889.
[13] S.A. Howard, K.D. Preston, Profile fitting of powder diffraction latterns, in: P.H. Ribbe (Ed.), Reviews in Mineralogy, vol. 20, Mineralogical Society of America, Washington, 1989„ , pp. 217–275(Chapter 8, Modern Powder Diffraction).
[14] Y. Tsur, T.D. Dunbar, C.A. Randall, Crystal and defect chemistry of rare earth cations in $BaTiO_3$, J. Electroceram. 7 (2001) 25–34.
[15] V.M. Goldschmidt, Die Gesetze der Kristallochemie, in: J. Dybwad (Ed.), Geochemische Verteilungsgesetze der Elemente (I–VIII), vol. VII, Norske Videnskaps-Akademi Kristiania, Oslo, 1926 , pp. 1–116.
[16] R.D. Shannon, Revised effective radii and systematic studies of interatomic distancesin halides and chalcogenides, Acta Crystallogr. A A32 (1976) 751–767.